Chemistry of gold(I, III) complexes with organic ligands as potential MOCVD precursors for fabrication of thin metallic films and nanoparticles

BASOVA, T.V., HASSAN, Aseel <http://orcid.org/0000-0002-7891-8087> and MOROZOVA, N.B.

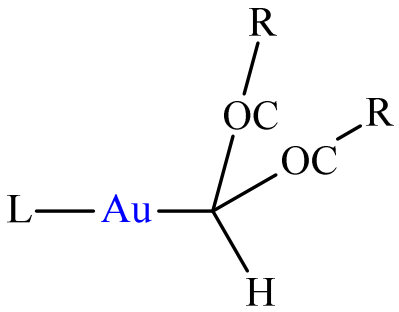

Fig. 1. Structure of gold(I) β-diketonates.

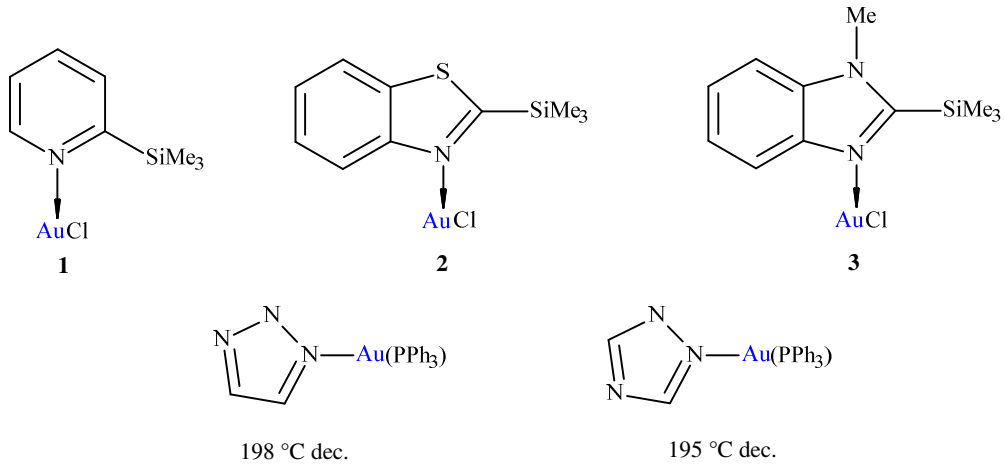

Fig. 2. Pyridine (**1**), benzothiazole (**2**) and benzoimidazole derivatives of gold chloride and complexes of (triphenylphosphine)gold with 1,2,3- and 1,2,4-triazole.

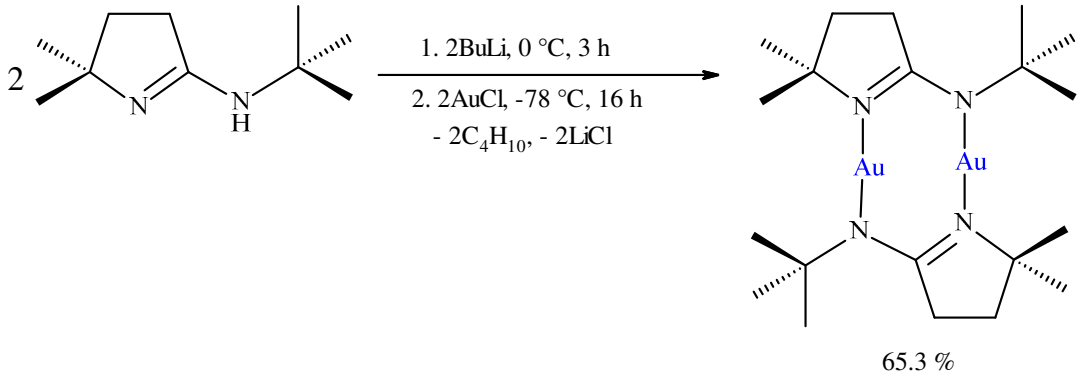

Fig. 3. Scheme of preparing gold(I) tert-butyl-imino-2,2-dimethylpyrrolidinate.

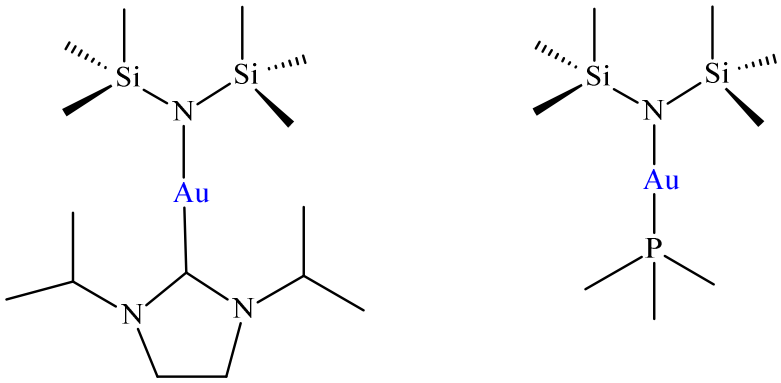

Fig. 4. Compounds Au(HMDS)(NHC) (**1**) and Au(HMDS)(PMe_3) (**2**).

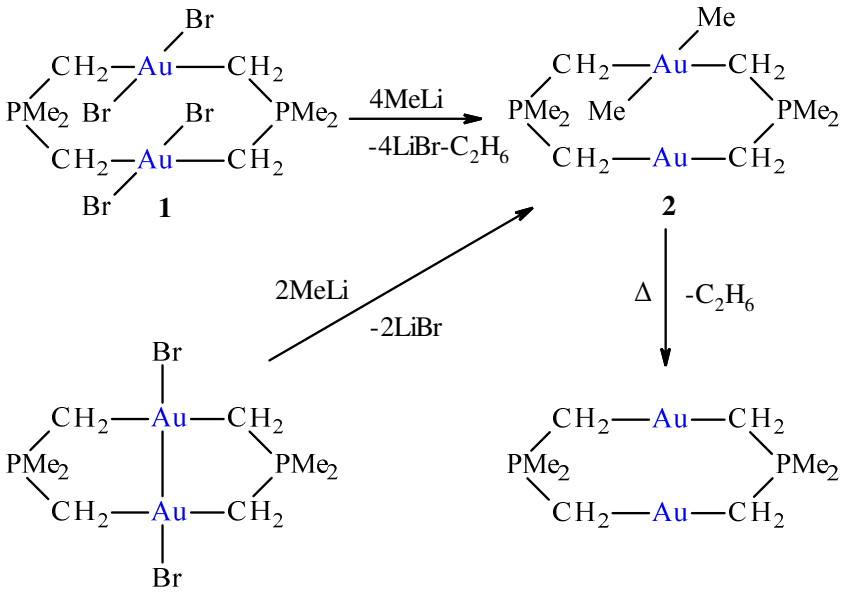

Fig. 5. The reactions of methyllithium with halogenated derivatives of dimer ylides.

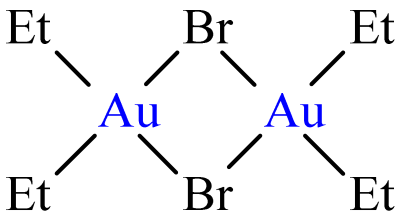

Fig. 6. Diethylgold(III) bromide.

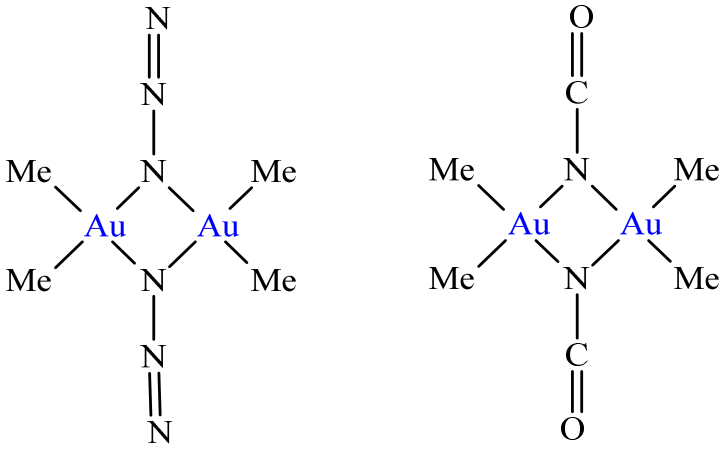

Fig. 7. Azide and cyanate of dimethylgold(III).

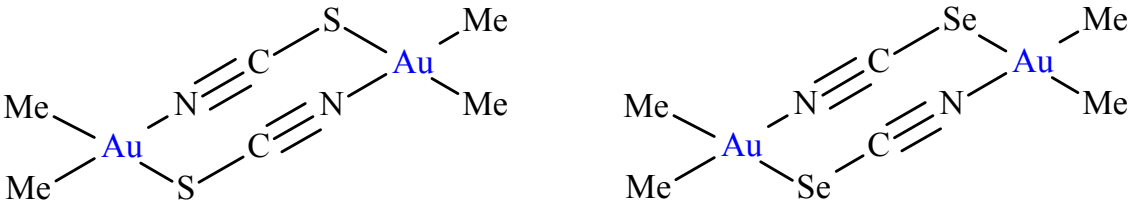

Fig. 8. Thio- and selenocyanate of dimethylgold(III).

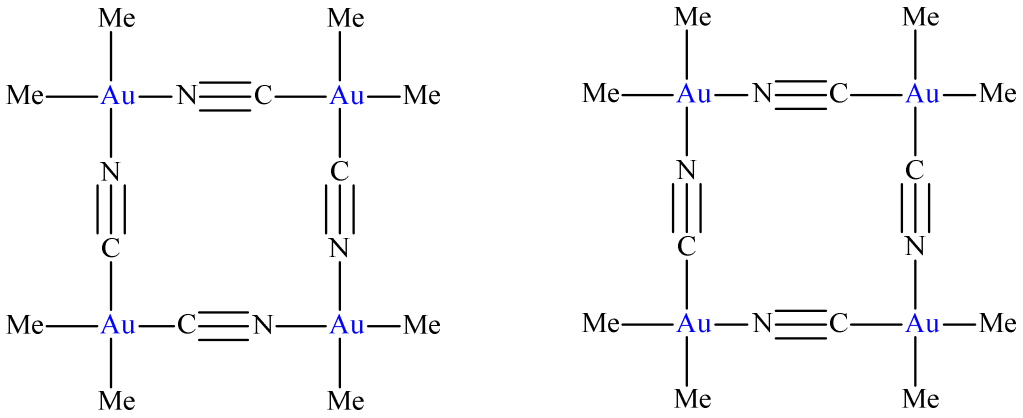

Fig. 9. Cyanides of dimethylgold(III).

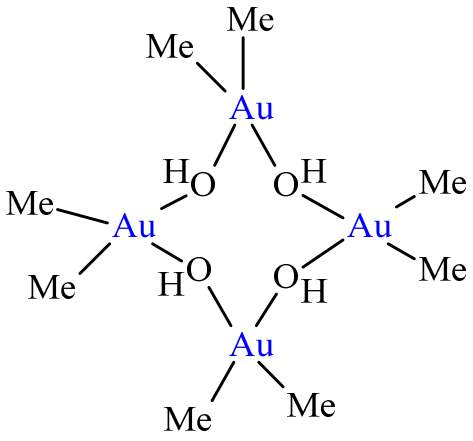

Fig. 10. Structure of dimethylgold(III) hydroxide.

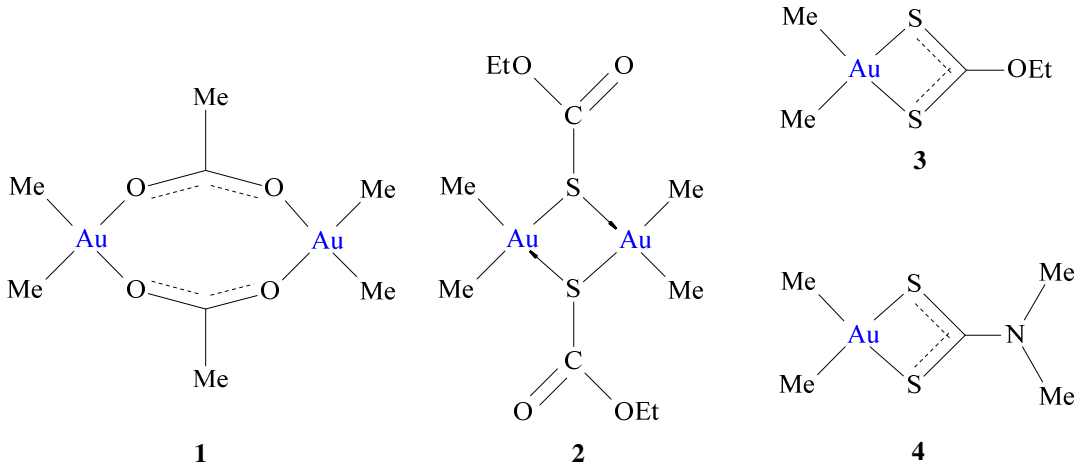

Fig. 11. Complexes of dimethylgold(III) with O- and S-donor ligands.

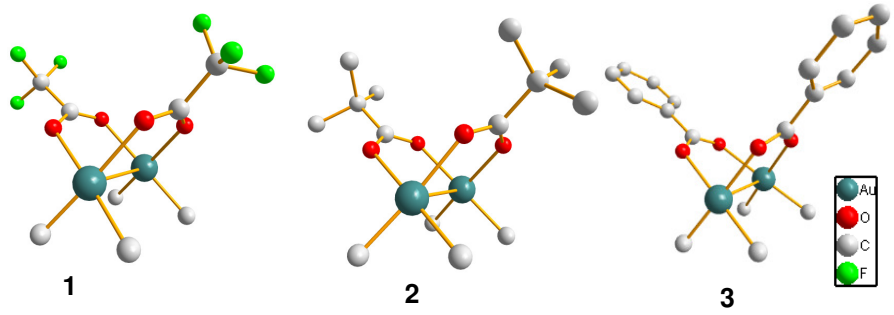

Fig. 12. Structure of dimethylgold(III) carboxylates $[Me_2Au(OOCR)]_2$ with R = CF_3 (**1**), *t*-Bu (**2**), Ph (**3**).

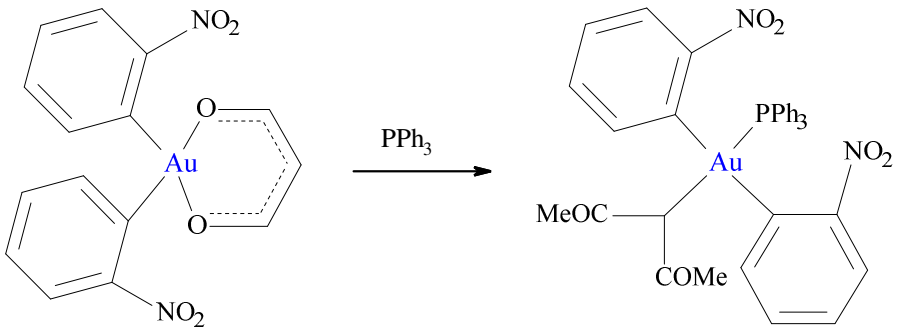

1 **2**

Fig. 13. The transformation of β-diketonates stabilized by orto-nitrobenzene radicals under the action of triphenylphosphine.

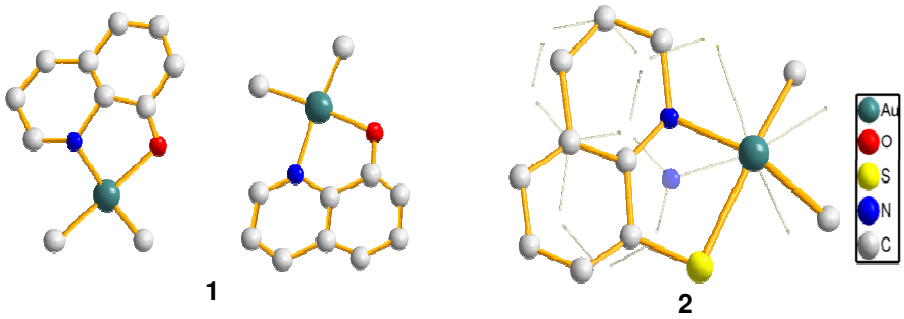

1 **2**

Fig. 14. Structure of $Me_2Au(ox)$ (**1**) and $Me_2Au(tox)$ (**2**).

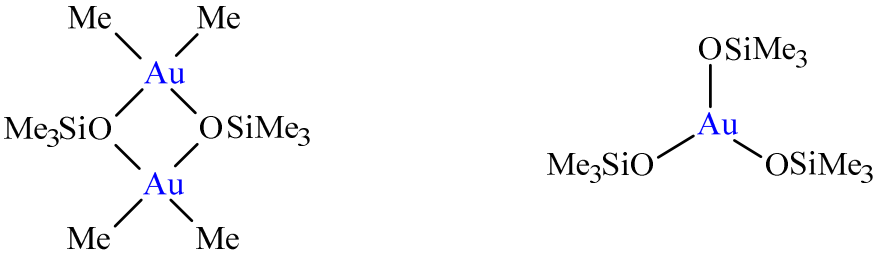

1 **2**

Fig. 15. Gold(III) complexes with trimethylsiloxy group.

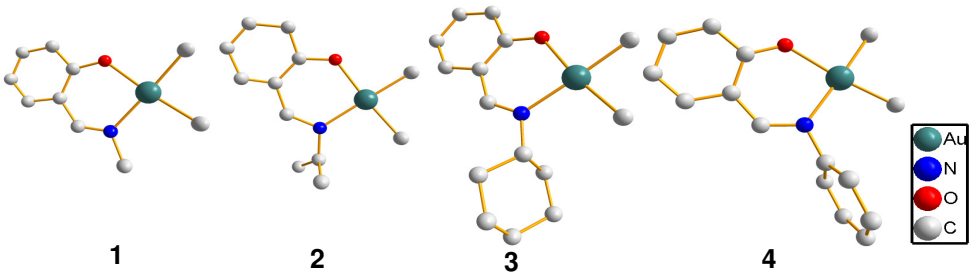

Fig. 16. Structures of $Me_2Au(Sal{=}NMe)$ (**1**), $Me_2Au(Sal{=}N(i\text{-}Pr))$ (**2**), $Me_2Au(Sal{=}NCy)$ (**3**), and $Me_2Au(Sal{=}NPh)$ (**4**).

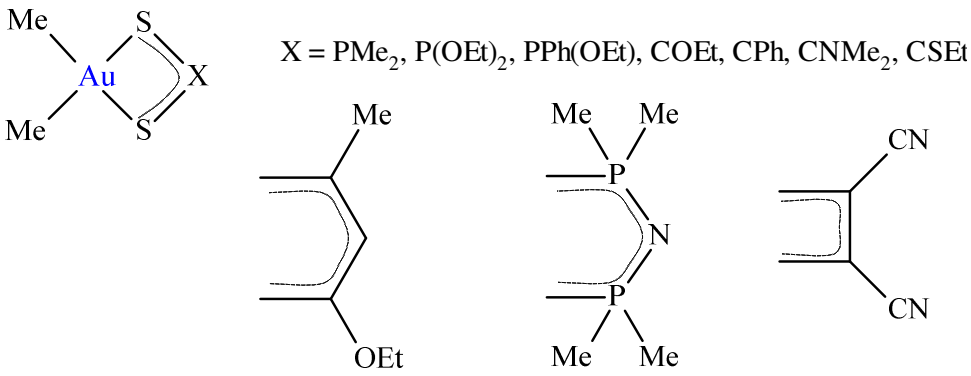

Fig. 17. Dimethylgold(III) compounds stabilized by S atom.

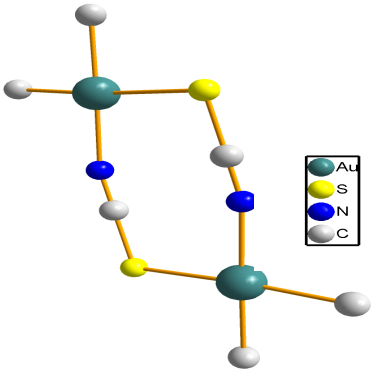

Fig. 18. Molecular structure of $[Me_2AuSCN]_2$.

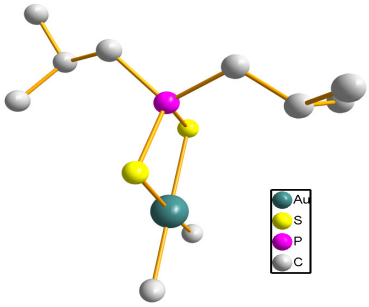

Fig. 19. Molecular structure of $Me_2AuS_2P(i\text{-}Bu)_2$.

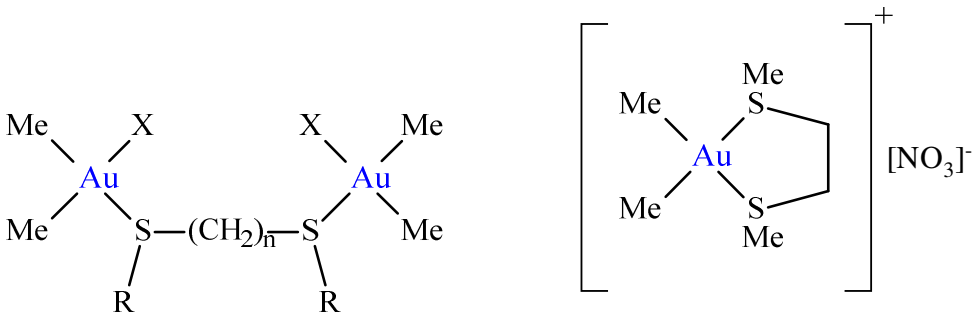

Fig. 20. Dimer (**1**) and monomer (**2**) thiocomplexes of dimethylgold(III).

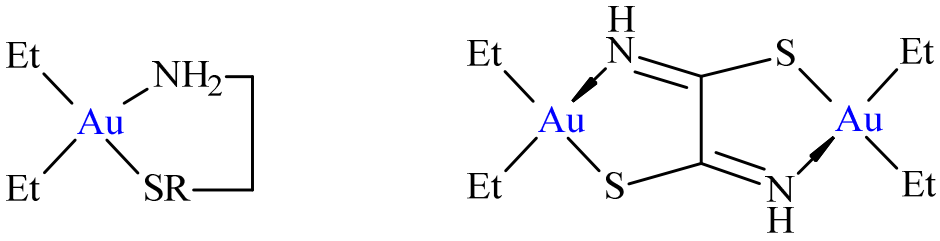

Fig. 21. Complexes of diethylgold(III) with N,S-coordination.

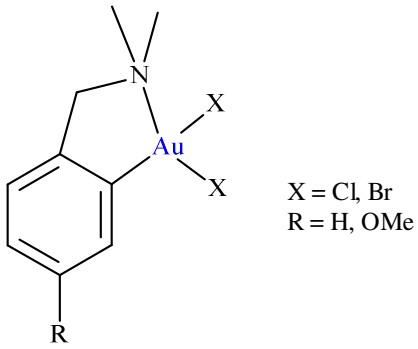

Fig. 22. Gold complexes with N,N-dimethylbenzylamine.

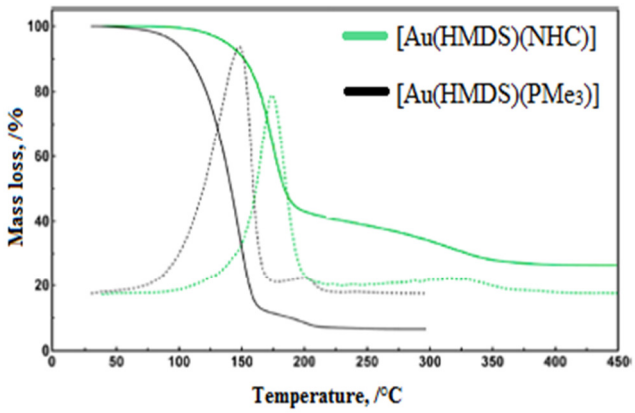

Fig. 23. TGA experiments of Au(HMDS)(NHC) (green) and Au(HMDS)(PMe_3) (black) are shown as solid lines. Derivative curves are shown by dashed lines. Reprinted with permission from Ref. [85]. Copyright 2015 American Chemical Society.

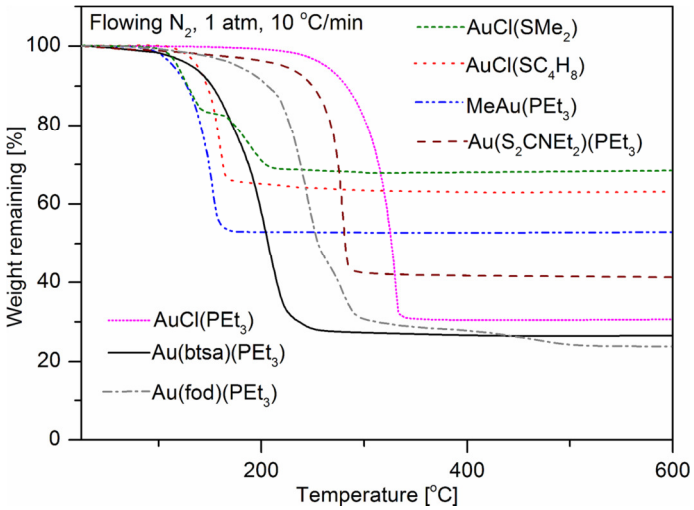

Fig. 24. TGA curves of Au compounds. Reprinted from Ref. [76] with permission from American Vacuum Society, Copyright 2017.

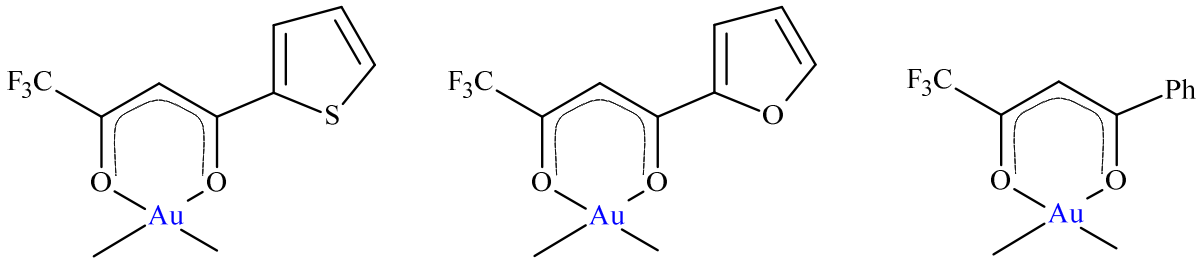

Fig. 25. Dimethylgold(III) β-diketonates: $Me_2Au(ttfac)$ (**1**) (ttfac - 1-(2-thienyl)-4,4,4-trifluoro-1,3-butanedionate), $Me_2Au(ftfac)$ (**2**) (ftfac - 1-(2-furanyl)-4,4,4-trifluoro-1,3-butanedionate), $Me_2Au(btfac)$ (**3**) (btfac - 1-phenyl-4,4,4-trifluoro-1,3-butanedionate).

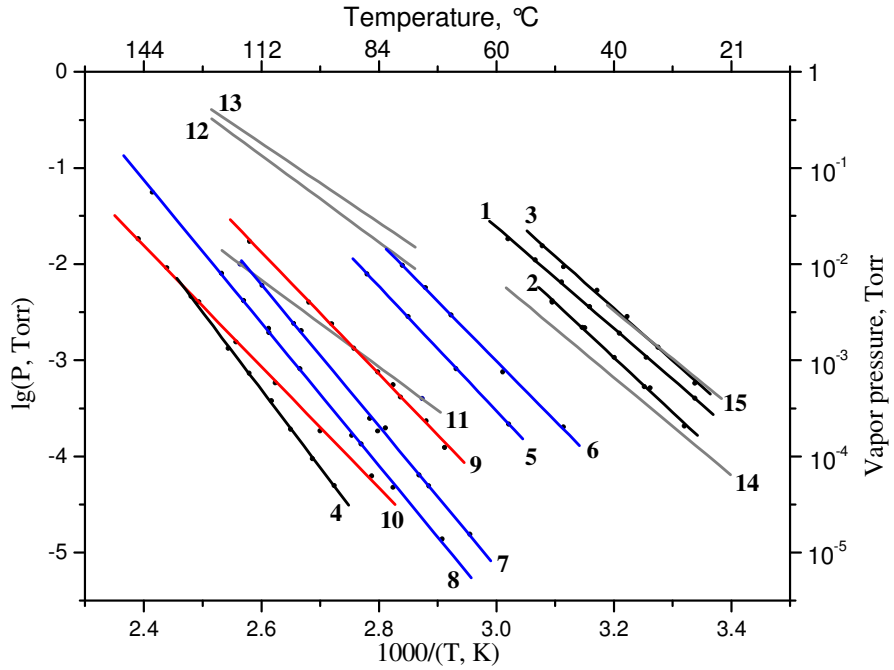

Fig. 26. *P*/*T* dependence for volatile complexes of dimethyigold(III) with organic ligands: **1** – $[Me_2Au(OAc)]_2$; **2** – $[Me_2Au(Piv)]_2$; **3** – $[Me_2Au(OOCCF_3)]_2$; **4** – $[Me_2Au(OBz)]_2$; **5** – $Me_2Au(Sal{=}N{-}Me)$; **6** – $Me_2Au(Sal{=}N{-}i\text{-}Pr)$; **7** – $Me_2Au(Sal{=}N{-}Cy)$; **8** – $Me_2Au(Sal{=}N{-}Ph)$; **9** – $Me_2Au(OQ)$; **10** – $Me_2Au(SQ)$; **11** – $Me_2Au(bac)$; **12** – $Me_2Au(ttfac)$; **13** – $Me_2Au(btfac)$; **14** – $Me_2Au(i\text{-}acac)$; **15** –$Me_2Au(acac)$ [117, 138-140, 147-149].

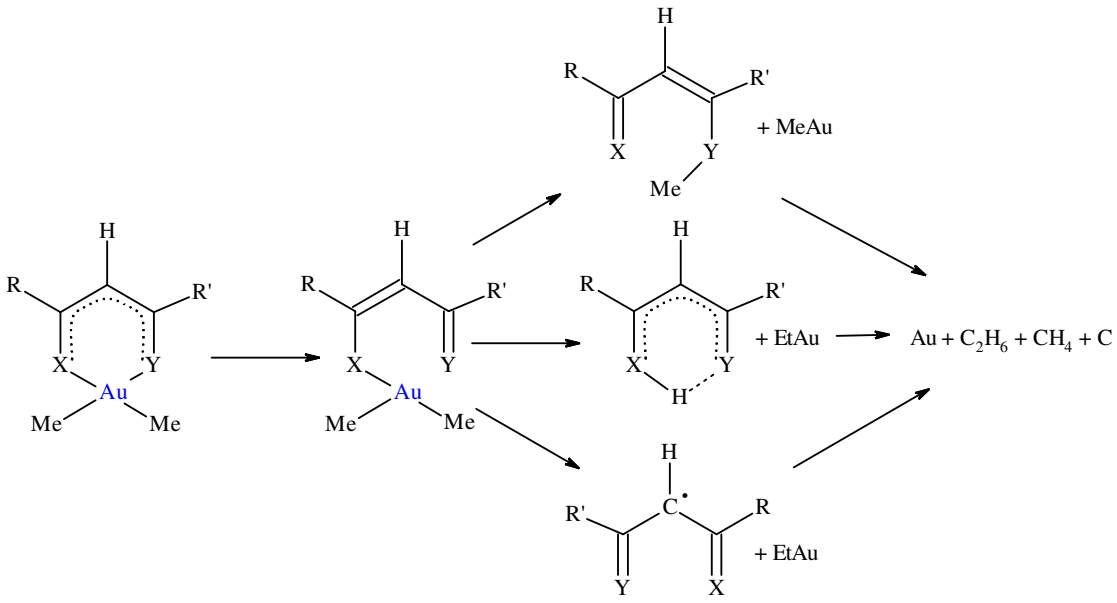

Fig. 27. Scheme of the thermolysis of dimethylgold(III) chelate vapors [112, 136].

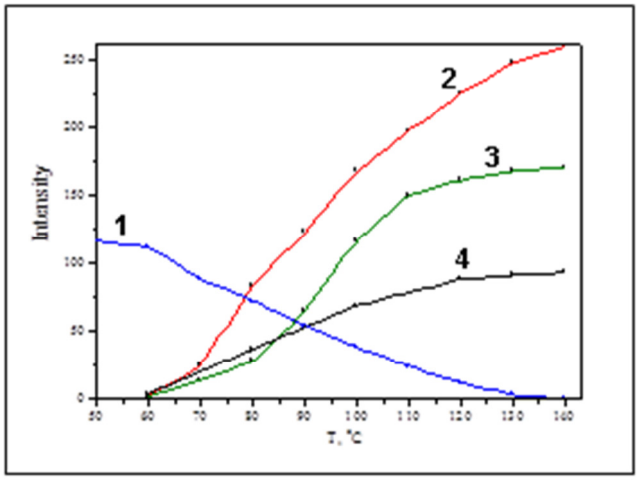

Fig. 28. Temperature dependence of the intensities of ion peaks of main gaseous products of thermal decomposition in the mass spectra of $[Me_2Au(OAc)]_2$: (a) – $[Au_2(OOCCH_3)]^+$, (b) – $[COCH_2]^+$, (c) – $[OOCCH_3]^+$, (d) – $[C_2H_6]^+$. Adapted by permission from Ref. [139] Springer Customer Service Centre GmbH, Nature Springer, Copyright 2008.

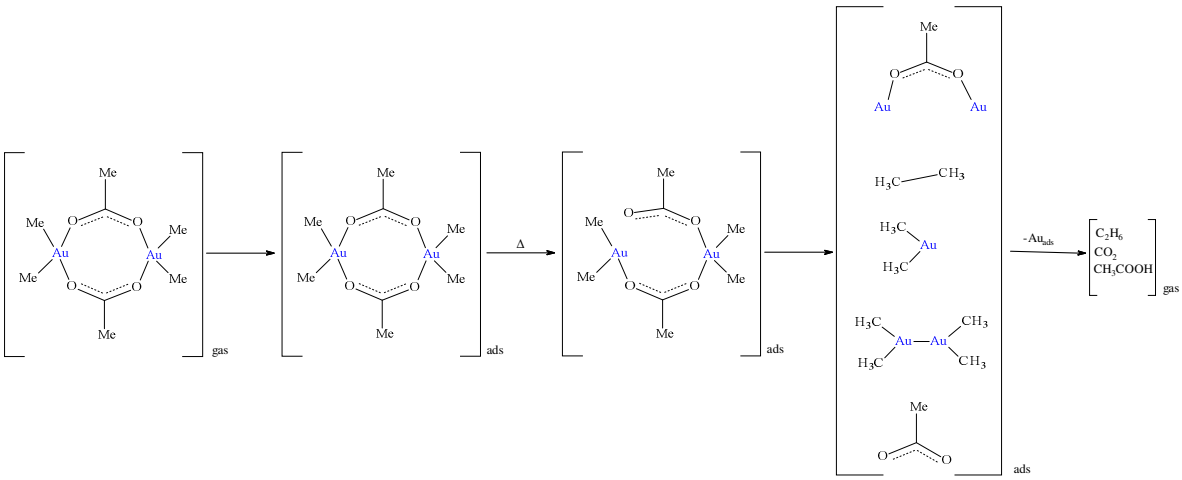

Fig. 29. Scheme of the chemical transformation of $[Me_2Au(OAc)]_2$ vapors on a heated surface in vacuum [138, 139].

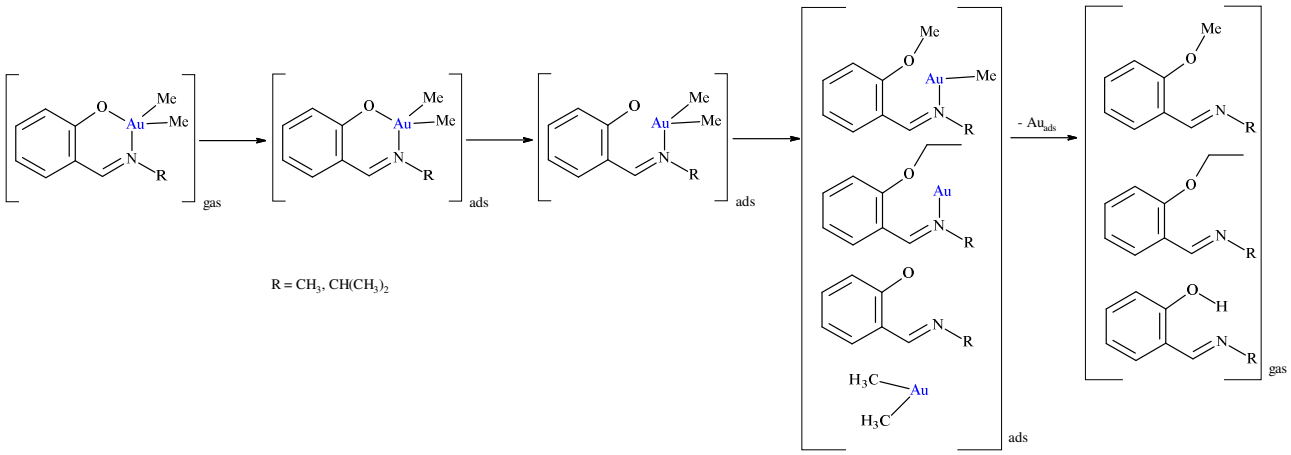

Fig. 30. Scheme of the chemical transformation of the vapors of dimethylgold(III) complexes with salicylaldimine on a heated surface in vacuum [117].

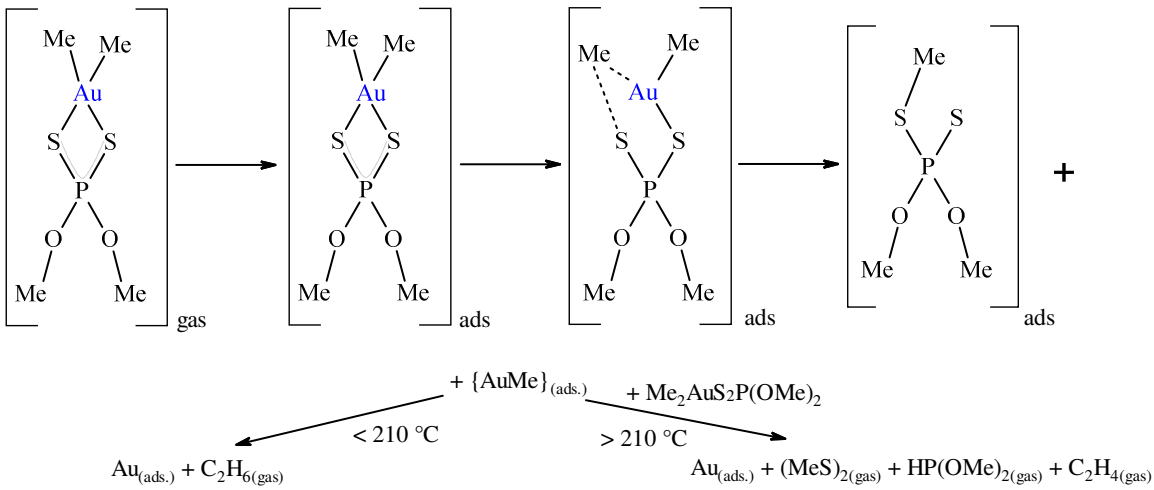

Fig. 31. Mechanism of thermal decomposition of $Me_2AuS_2P(OMe)_2$.

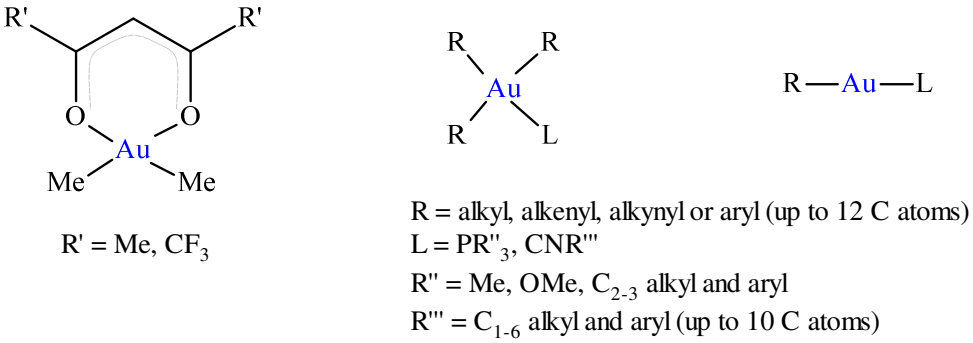

Fig. 32. Volatile gold complexes for CVD processes [93, 162].

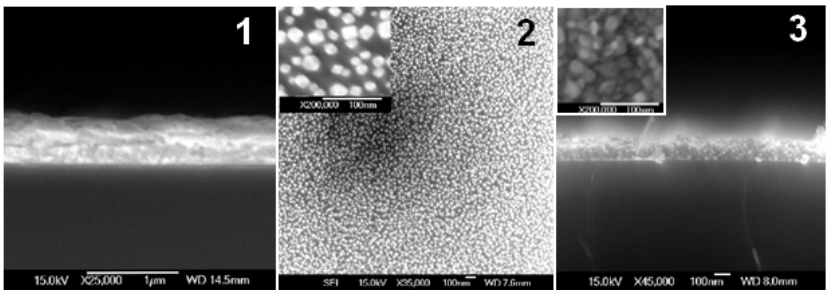

Fig 33. SEM images of gold coatings on Si(100) deposited using $[Me_2Au(OAc)]_2$ (**1**), $Me_2Au(Sal{=}N{-}Me)$ (**2**) and $Me_2Au(Sal{=}N{-}i\text{-}Pr)$ (**3**) as precursors. Adapted from Ref. [138] with permission from Elsevier, Copyright 2007.

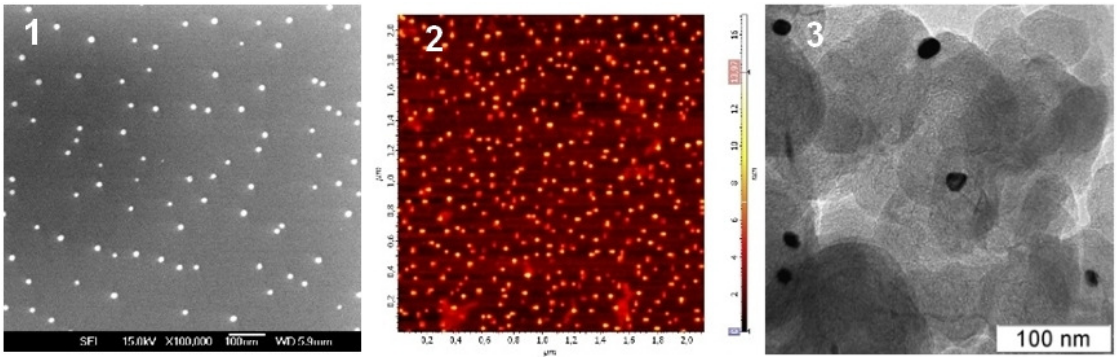

Fig. 34. SEM (**1**), AFM (**2**) and TEM (**3**) images of gold nanoparticles deposited by pulse-CVD on the surface of nanocarbon [171].

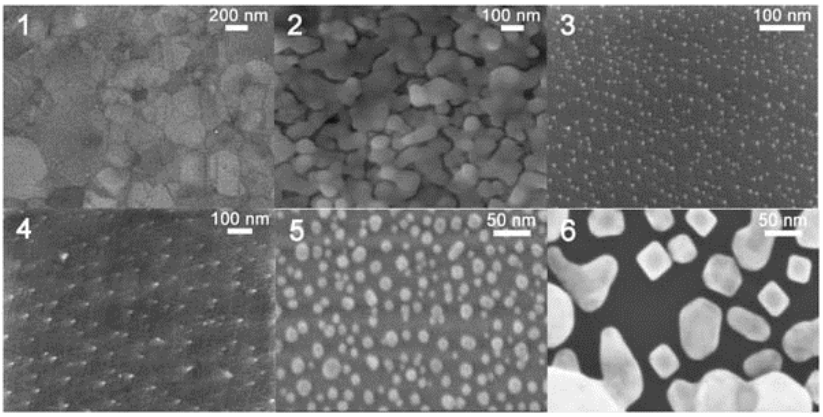

Fig. 35. SEM images of gold films and nanoparticles deposited under similar conditions from different precursors: $[Me_2Au(OAc)]_2$ (**1**), $Me_2Au(Piv)$ (**2**), $Me_2Au(OQ)$ (**3**), $Me_2Au(SQ)$ (**4**), $Me_2Au(thd)$ (**5**), $Me_2Au(S_2CNEt_2)$ (**6**). Reprinted with permission from Ref. [172]. Copyright 2012 John Wiley and Sons.

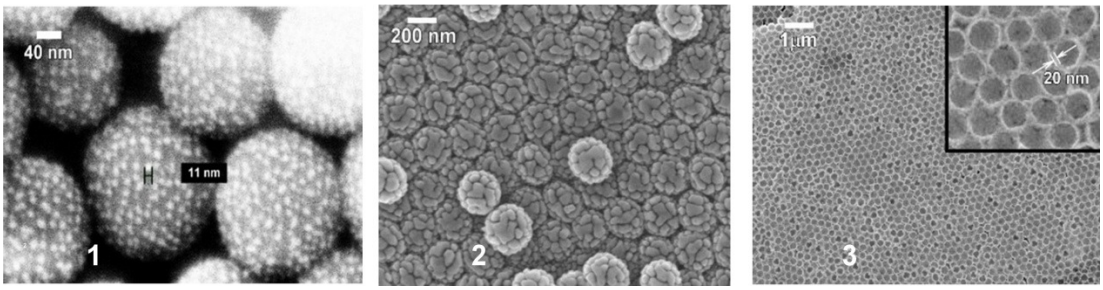

Fig. 36. SEM images of gold nanoparticle (**1**) and thin films (**2**) deposited onto the matrix of photonic crystals as well as hollow gold nanoshells (**3**). Reprinted from Ref. [173] with permission from Elsevier, Copyright 2013.

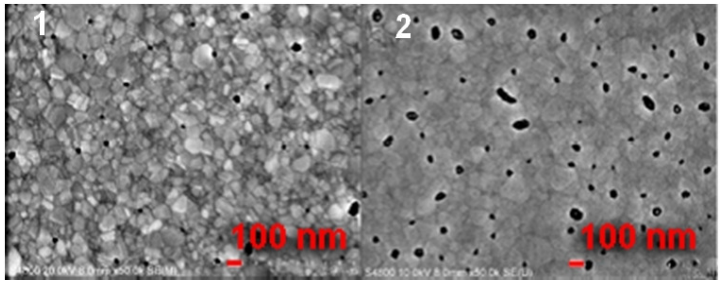

Fig. 37. FESEM images of Au films deposited with 0.5 s (**1**) and 2 s (**2**) $Me_2Au(S_2CNEt_2)$ pulses at 180°C. The O_3 pulse was 1 s. Adapted with permission from Ref. [143]. Copyright (2017) American Chemical Society.

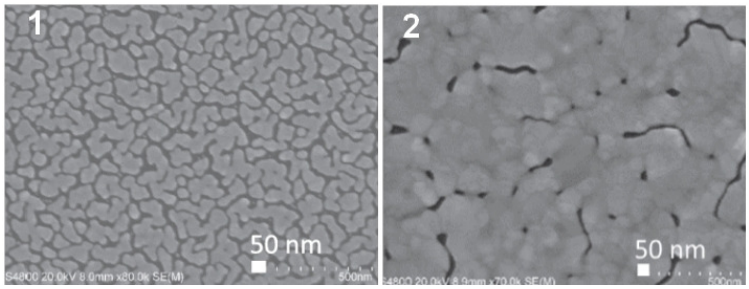

Fig. 38. FESEM images of Au thin films (**1**) and thick films (**2**). Reprinted from Ref. [76] with permission from American Vacuum Society, Copyright 2017.